A UNIFIED APPROACH TO JOINT REGIONAL/TELESEISMIC CALIBRATION AND EVENT LOCATION WITH A 3D EARTH MODEL

William L. Rodi[1], Delaine T. Reiter[2], Stephen C. Myers[3], and Nathan A. Simmons[3]

Massachusetts Institute of Technology[1], Weston Geophysical Corporation[2], and
Lawrence Livermore National Laboratory[3]

Sponsored by the National Nuclear Security Administration

Award Nos. DE-AC52-08NA28539[1, 2] and DE-AC52-07NA27344[3]
Proposal No. BAA08-19

ABSTRACT

This project is investigating the problem of locating seismic events from combined data sets of regional and teleseismic arrival times, based on the use of a unified 3D model of the Earth's velocity structure to predict travel times for both types of data. Inherent to this problem is the joint tomographic calibration of the Earth model with both regional and teleseismic ground-truth data. The goal of the unified approach is to remove the inconsistencies that result when travel-time predictions are performed with a mixture of separately calibrated regional and global models and empirical corrections, which can lead to degradation in event location accuracy. Additionally, the unified approach provides a rigorous framework for choosing optimal relative weighting of different types of data used in locating an event.

We are addressing a number of practical difficulties that arise in the pursuit of a unified location/calibration capability. One is to develop fast and accurate raytracing techniques for modeling different types of seismic arrivals. A second is the computational challenge of performing joint tomographic calibration with very large numbers of data and model parameters. We are considering various strategies for reducing the problem size, such as averaging data from proximate events and stations, and for breaking the calibration problem into equivalent sub-problems by region or depth range. The calculation of model uncertainty, and its translation to travel-time prediction uncertainty, provides optimal data weighting for locating events, but adds greatly to the computational challenge.

A significant computational savings, in both calibration and location, is achieved by employing a linearized approximation to travel-time calculations, obtained by integrating the slowness function of a 3D model along ray paths computed in a 1D reference model. While this approximation is not adequate for regional travel times, we have performed numerical experiments that indicate it is quite accurate for teleseismic travel times, as judged by comparing to travel times calculated with a highly accurate raybending method. We have also continued numerical experiments, initiated last year, with joint regional/teleseismic travel-time tomography built on the linearized forward model for teleseismic data. The results to date indicate that biases between regional and teleseismic travel-time predictions, which create difficulties for an event location algorithm, are removed by the joint calibration process.

OBJECTIVE

Previous studies have demonstrated that 3D models of crust and upper mantle velocity structure predict significantly more accurate travel times for regional seismic phases than do 1D global models, leading to more accurate locations for small, regionally recorded events (e.g., Ryaboy et al., 2001; Murphy et al., 2005; Flanagan et al., 2007; Reiter and Rodi, 2009). However, it is not uncommon to also observe teleseismic arrivals from small events of monitoring interest, at least in part of the teleseismic distance range. While adding teleseismic to regional data should in theory improve event locations even further, it has not always been the case in practice. For example, Yang et al. (2004) found that event locations obtained by combining regional and teleseismic data were only more accurate than locations found from the separate data sets if they corrected for a bias between teleseismic and regional travel-time predictions, each made from a different 3D model: CUB1.0 (Ritzwoller et al., 2002) for regional, and J362D28 (Antolik et al., 2003) for teleseismic. The correction they inferred is small (0.79 s), but even small, systematic shifts in teleseismic travel times can induce large location errors owing to the high apparent velocity of teleseismic waves.

We are investigating a methodology for seismic event location based on the principle that travel times for all seismic phases should be predicted consistently with a single 3D Earth model. This unified modeling approach would be applied as the forward model in locating events from combined sets of regional and teleseismic data. Moreover, the 3D model would be calibrated with regional and teleseismic ground-truth data in a joint tomographic analysis. A unified approach to location and travel-time calibration is not a new concept and, in fact, has been the approach taken with 1D Earth modeling for many decades. Applying the approach to 3D Earth models, however, presents many strategic and computational challenges, which this project is attempting to address.

RESEARCH ACCOMPLISHED

Our project is focusing on the development of a prototype capability for event location and travel-time calibration with 3D Earth models, applicable to regional and teleseismic data. Our goal is not to develop a complete and operations-ready 3D capability but rather to demonstrate the value and practicality of the unified approach. The following sections describe our progress to date in developing two key components of the approach: 3D travel-time calculation and joint regional/teleseismic tomography.

Travel-Time Linearization

A number of numerical methods are available for raytracing and travel-time calculation in 3D Earth models, such as the finite-difference eikonal method (e.g., Podvin and Lecomte, 1991), fast marching (Rawlinson and Sambridge, 2004), and two-point raybending (e.g., Um and Thurber, 1987). Given the computational intensity of these full 3D methods, many applications, such as global tomography with teleseismic data, have used approximate travel times calculated with linearization around a 1D reference model. In this approximation, the travel time T through a 3D model of interest is obtained by integrating the model's slowness function along the Fermat raypath computed in a different, reference model velocity model:

$$T \approx \int d\mathbf{x}\, a(\mathbf{x}; v_{\mathrm{ref}})\, v^{-1}(\mathbf{x}) \qquad (1)$$

where $\mathbf{x}$ is the position vector; $v(\mathbf{x})$ is the 3D velocity function of interest; and $a(\mathbf{x}; v_{\mathrm{ref}})$ is a sensitivity distribution concentrated on the Fermat raypath evaluated in the reference velocity function, $v_{\mathrm{ref}}(\mathbf{x})$. When $v_{\mathrm{ref}} = v$, T is exact. When v_{ref} is 1D, linearization of travel times offers great computational advantages in both computation time and storage. It also greatly simplifies the computation of times for secondary arrivals.

Rodi et al. (2009) conducted a preliminary investigation of the accuracy of travel-time linearization in 3D velocity models. Their experiments involved the computation of P-wave travel times for various paths in southern Asia through the JWM model of Reiter and Rodi (2009). Linearized times, using reference rays for model AK135 (Kennett et al., 1995), were compared to travel times calculated with the Podvin-Lecomte (P-L) finite-difference method, with the presumption that the latter are more accurate and can be used to judge the adequacy of linearization. The numerical tests reported last year showed that linearization about AK135 was very inaccurate for computing travel times at regional distances, as expected, but seemed to be a good approximation at teleseismic distances except for some bothersome artifacts related to shallow velocity structure. The tests were not definitive, however, because the accuracy of the

P-L times, which are also approximate, was not known. Moreover, the JWM model is the same as AK135 below a depth of 410 km, weakening the tests.

We have continued this investigation of travel-time linearization with the aim of getting a more definitive assessment of its accuracy. The new tests we report here involve three main changes from our preliminary tests. First, the calculations were performed with the 3D velocity model taken to be a portion of Lawrence Livermore National Laboratory's (LLNL's) recently developed G3D-LLNL global tomographic model (Simmons et al., 2010), which has 3D velocity anomalies throughout the crust and mantle. Second, we modified our algorithm for computing linearized travel times to be more accurate when reference rays traverse low velocity, shallow layers in the 3D model.

In a third departure from our earlier investigation, we used highly accurate raybending calculations as the benchmark for assessing the accuracy of linearization. The raybending calculations through G3D-LLNL were performed by LLNL using an algorithm they adapted from the 3D raytracing procedure of Zhao (1992) and Zhao and Lei (2004). This technique combines the pseudo-bending method for continuous media, developed by Um and Thurber (1987), and refraction (Snell's law) at velocity discontinuities. The specific approach is outlined in Simmons et al. (2009).

Our new tests considered travel times between various station locations and a 3D grid of event locations. The event grid covers the box 15°–55° N, 30°–80° E (roughly, the Middle East) at 1° spacing, but contains only a few event depths between the surface and 120 km. We performed calculations for four station locations, one at each corner of the event grid and each at zero depth. We will refer to these as Station NW, etc.

Figure 1 compares travel times calculated through G3D-LLNL (with raybending) to those calculated through AK135. We see that the effects of 3D velocity structure in G3D-LLNL on regional times is several seconds. The 3D effects on teleseismic travel times (distance greater than ~23 deg) are smaller but still significant. For the same stations and grid of surface events, Figure 2 shows the discrepancy between travel times calculated through G3D-LLNL with raybending and with linearization around AK135, i.e. integrating the slowness function of G3D-LLNL along rays generated in AK135. Given the high accuracy of the raybending method, the travel-time discrepancy plotted in Figure 2 can be interpreted as the error in the linearization calculations. The same results are shown geographically in Figure 3.

Figures 2 and 3 demonstrate that the errors in linearized Pn times can be very large, as much as 30 s for some paths (not seen in the plots due to clipping). The errors at teleseismic distances are much smaller, being generally well below 0.5 s. However, it is notable in Figure 3 that the largest errors in linearized times for these surface events correlate with the areas having the lowest near-surface velocities, i.e. the oceans. For deeper events, the surface-related artifacts disappear (Figure 4). While in practice we do not need to be concerned with event locations in oceans and slow sediments, we are still investigating whether our ray integration scheme may be undersampling thin, low velocity layers in the 3D model, or whether we have simply reached a situation in which linearization is not adequate.

Figures 2–4 also show that the errors in linearized teleseismic times are predominantly negative, which seemingly violates Fermat's Principle. One explanation for the negative bias is a quirk in our experiments whereby the effects of the Earth's ellipticity were calculated differently in the raybending and linearization methods. We may also be seeing the above-mentioned problems with thin, low-velocity layers beneath the stations (rather than the events).

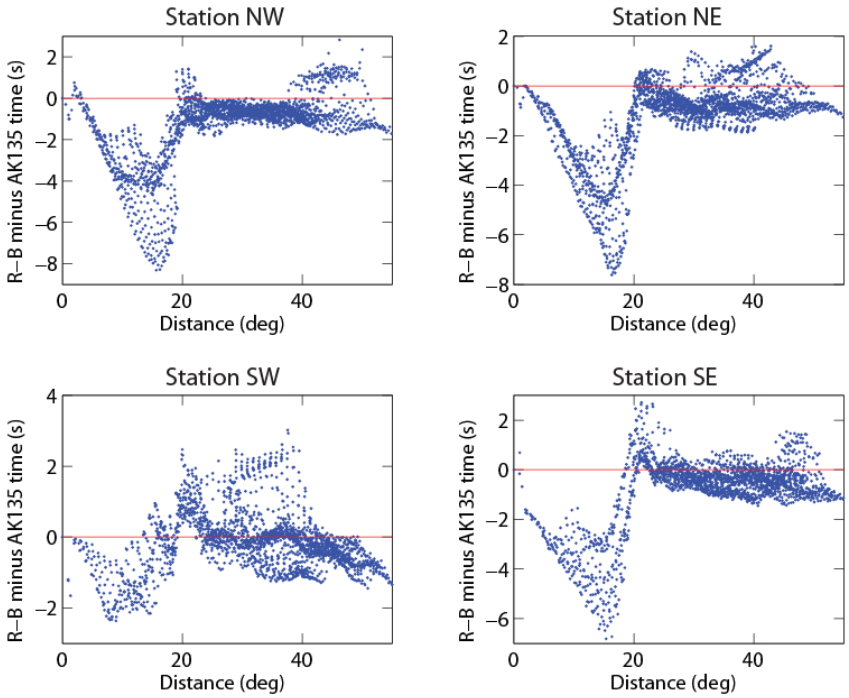

Figure 1. Difference between travel times through models G3D-LLNL and AK135, calculated between each of four stations and a grid of surface events. The G3D-LLNL times were calculated with raybending; AK135 times were calculated analytically. The time differences are plotted as a function of epicentral distance.

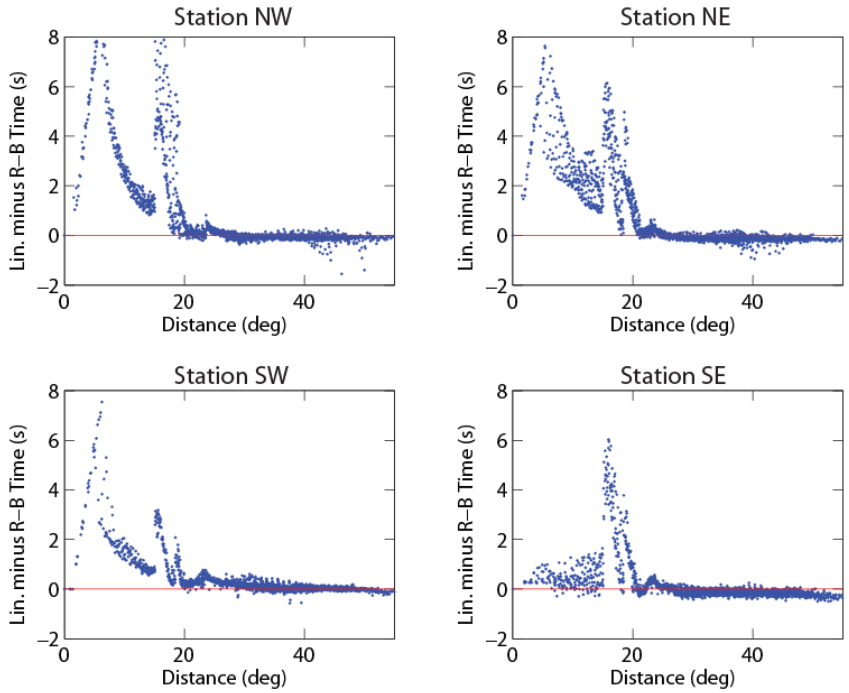

Figure 2. Discrepancy between travel times calculated through model G3D-LLNL with two methods: raybending and linearization relative to AK135 rays. Each panel shows the discrepancy vs. distance for paths from one of the corner stations to the geographic grid of surface events. The travel-time scale has been clipped at 8 sec.

Joint Regional/Teleseismic Tomography

Rodi et al. (2009) reported on preliminary tests of joint regional/teleseismic calibration, whereby the JWM model of southern Asia derived by Reiter and Rodi (2009) was updated through linearized tomography applied to a combination of regional and teleseismic P-wave travel times. Linearized tomography uses Equation (1) to model travel times. For teleseismic times, we take the reference velocity model to be AK135, which our numerical experiments have shown to be adequate. The same experiments showed that linearization about AK135 is not adequate for regional travel-time calculation; therefore, we used JWM as the reference model for regional times.

The regional data set used in the joint calibration tests was identical to that used by Reiter and Rodi (2009) in constructing JWM. Two teleseismic data sets were considered, both extracted from the EHB database (Engdahl et al., 1998) and both including arrivals only in the epicentral distance range 35°–65°. In the first teleseismic data set (termed TelE), the stations were restricted to be located in or near the JWM study region, i.e., in the box 0°–60° N, 30°–120° E. The event locations were unrestricted (except for the distance criterion) and fell primarily outside this box. The second data set (TelS) restricted the events to be within the study box and accepted all stations obeying the distance criterion. The regional and both teleseismic data sets included only events which have EHB focal depths less than 200 km and which are deemed well-located in accordance with criteria described by Reiter and Rodi (2009). To reduce the size and redundancy of the data sets, individual events were lumped into summary events in the same manner as done for JWM, with each summary event being a node on a 0.5° geographic grid and an irregular depth grid.

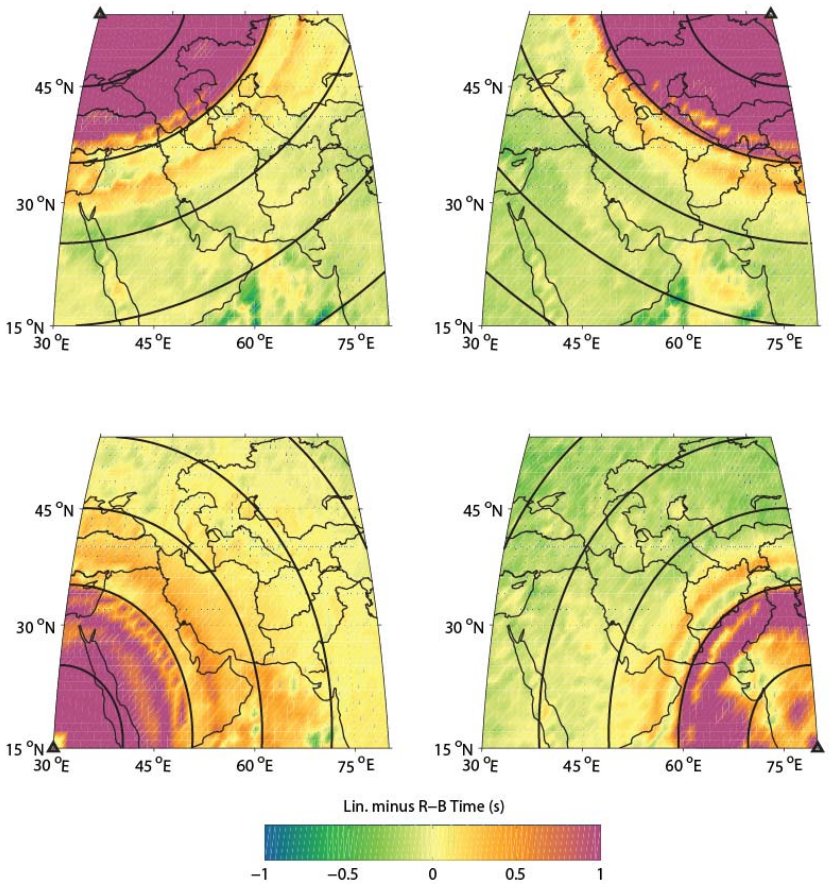

Figure 3. Discrepancy between travel times calculated through model G3D-LLNL with raybending and linearization. The discrepancies shown are the same as in Figure 2 but plotted as a function of the epicenter of the surface events. The travel-time scale has been clipped at -1 and +1 sec.

We have repeated these experiments using our improved algorithm for computing linearized travel times, and with upgraded teleseismic data sets. The teleseismic data were extracted from the updated EHB database distributed by the International Seismological Centre (http://www.isc.ac.uk/EHB/index.html). The new database included two additional years (2005 and 2006) as well as additional arrivals for years prior to 2005. After forming summary events, data set TelE contained 411,232 teleseismic P arrivals for 15,576 summary events and 900 stations. TelS contained 360,706 arrivals from 4,253 summary events and 2,846 stations. The teleseismic data sets are considerably larger than the regional data set, which contains 104,065 arrivals (>99% being the Pn phase) from 3,689 summary events and 603 stations. These data-set sizes approach the capacity of our current tomography software, which is why we considered teleseismic events and stations separately, and why we capped epicentral distances at 65°.

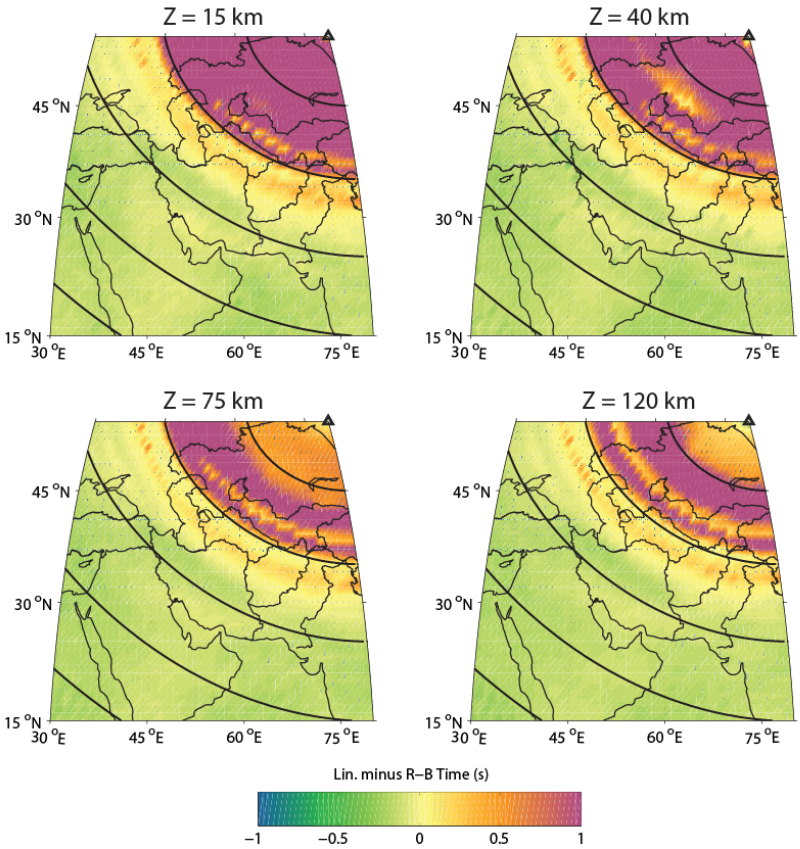

Figure 4. Discrepancy between travel times calculated through model G3D-LLNL with raybending and linearization. Each panel shows the discrepancy for paths from Station NE to a geographic grid of events at the labeled focal depth (*z*).

Figure 5 shows a vertical slice through each of two joint regional/teleseismic tomography models, corresponding to the two versions of the teleseismic data set that were combined with the common regional data set. The model obtained with TelE as the teleseismic data set is labeled JWM_TelE, and the other model as JWM_TelS. Both models are displayed as deviations from JWM. We see that the models are quite similar to each other, and overall have lower velocities than JWM. The largest differences from JWM occur at depths below 200 km, where the P velocity is significantly slower.

The reason for the lower mantle velocities in JWM_TelE and JWM_TelS is clear if we compare their travel-time residuals to those of JWM. Figure 6 displays separate histograms of regional (left) and teleseismic (right) residuals for each joint inversion model (red lines), compared in each case to the corresponding histograms for JWM (blue lines). We see that JWM yields regional residuals with a mean near zero but teleseismic residuals with a large positive mean: 1.8 s for the TelE residuals and 1.6 s for the TelS residuals. Both joint inversion models maintain the unbiased fit to the regional data and yields zero-mean teleseismic residuals as well. Each joint regional tomography

removed the teleseismic travel-time bias of JWM by lowering the P velocity below 200 km depth, in a way that preserved the fit to the Pn data.

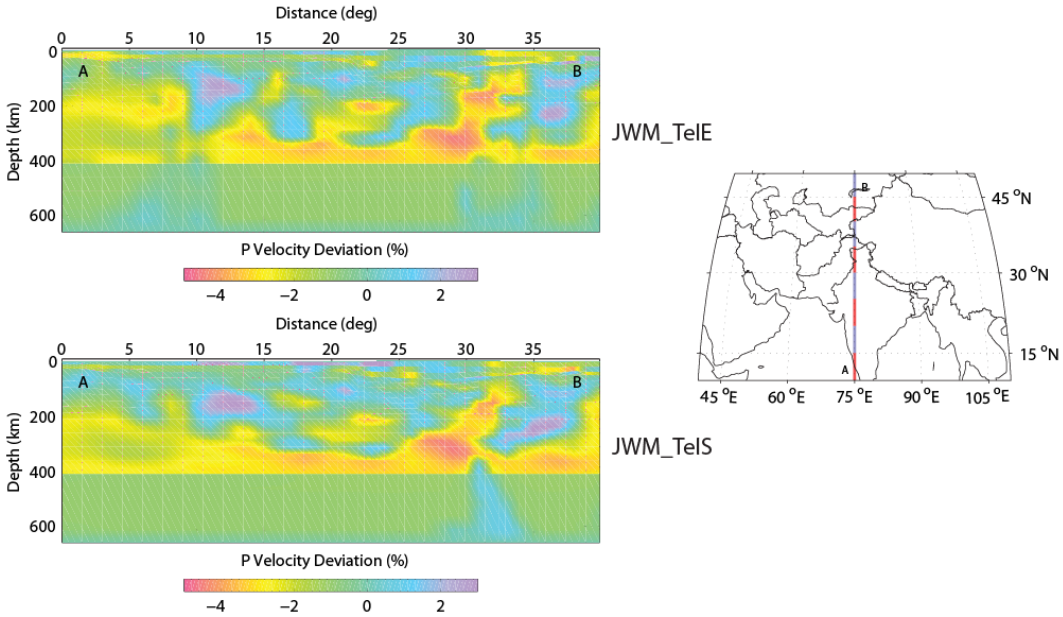

Figure 5. A vertical section through two 3D P velocity models obtained by joint inversion of regional and teleseismic P-wave travel times, each shown in terms of its velocity deviation from model JWM. The top model (JWM_TelE) used teleseismic data from local stations and teleseismic events, while the bottom model (JWM_TelS) used teleseismic data from local events and teleseismic stations. The regional data were the same in both cases and are from stations and events inside the model region. Note that the color scale for velocity deviation is asymmetrical (shifted toward negative deviations).

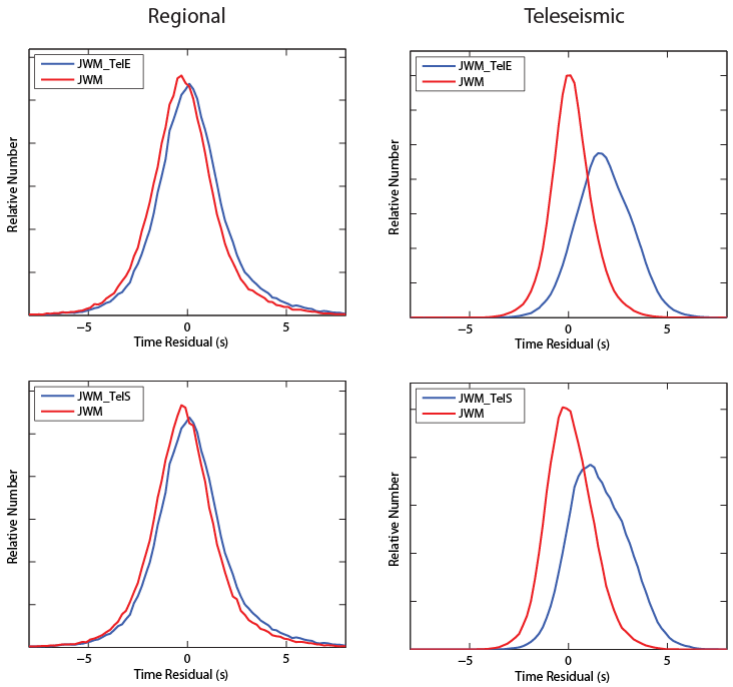

Figure 6. *Red lines*: Distributions of regional (left) and teleseismic (right) travel-time residuals for models JWM_TelE (top panels) and model JWM_TelS (bottom panels). The teleseismic data set is TelE (teleseismic events) for the top-right panel and TelS for the bottom-right panel. *Blue lines:* Analogous distributions for model JWM.

Joint Tomography with Hypocenter Relocation

The above tomography results and those presented in Rodi et al. (2009) do not account for the effect of event mislocations on the velocity model. We have addressed this by extending our tomography algorithm to allow event hypocenters and origin times to vary, in accordance with specified prior errors. We followed the approach developed by Spencer and Gubbins (1980) and Pavlis and Booker (1980), whereby a projection operator is applied to the travel-time residual vector and its sensitivity matrix to remove patterns in the residuals that can be explained by perturbing the hypocenters and origin times of the events. Departing from the original formulations of the approach in terms of matrix inversion, we implemented the projection operations within the conjugate gradients technique we use for computing tomographic models.

To test the new capability, we repeated the two joint regional/teleseismic tomography experiments of the previous section, allowing variable event locations with a prior hypocentral uncertainty of 10 km (epicenter and depth) and origin time uncertainty of 2 s (all at 95% confidence). Figure 7 shows a slice through the resulting inversion models (called JWM_TelE_loc and JWM_TelE_loc). We see that model JWM_TelE_loc deviates much less from JWM than did model JWM_TelE (Figure 5 top vs. Figure 7 top), showing that perturbations to the teleseismic event locations can fit a significant portion of the JWM residuals. Models JWM_TelS_loc and JWM_TelS are less different. However, as before, both joint inversion models reconcile the regional/teleseismic travel-time bias of JWM, as seen in Figure 8. We also see that the residual histograms for JWM_TelE_loc, and to a lesser extent JWM_TelS_loc, are more peaked than before as a result of allowing perturbations in the event locations.

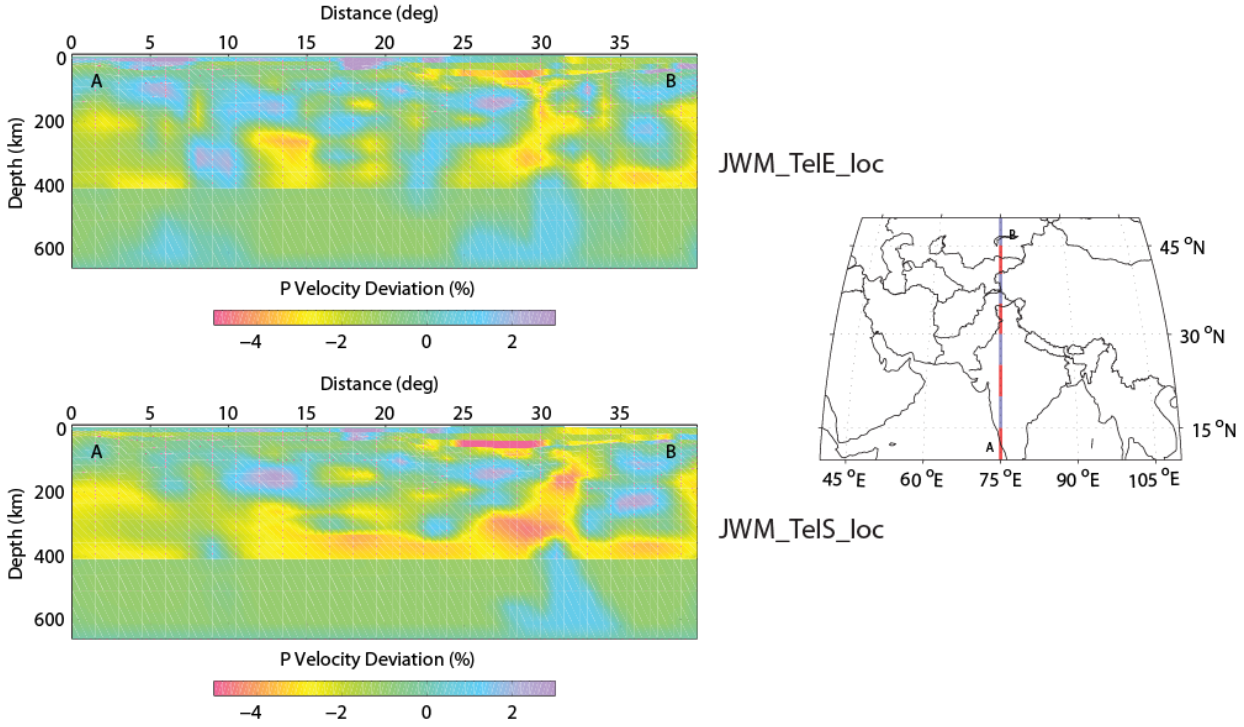

Figure 7. A vertical section through two 3D P velocity models (JWM_TelE_loc and JWM_TelS_loc) obtained by joint inversion of regional and teleseismic P-wave travel times, each shown in terms of its velocity deviation from model JWM. This figure is analogous to Figure 5 except that the joint inversion models were obtained in conjunction with linearized hypocenter relocation.

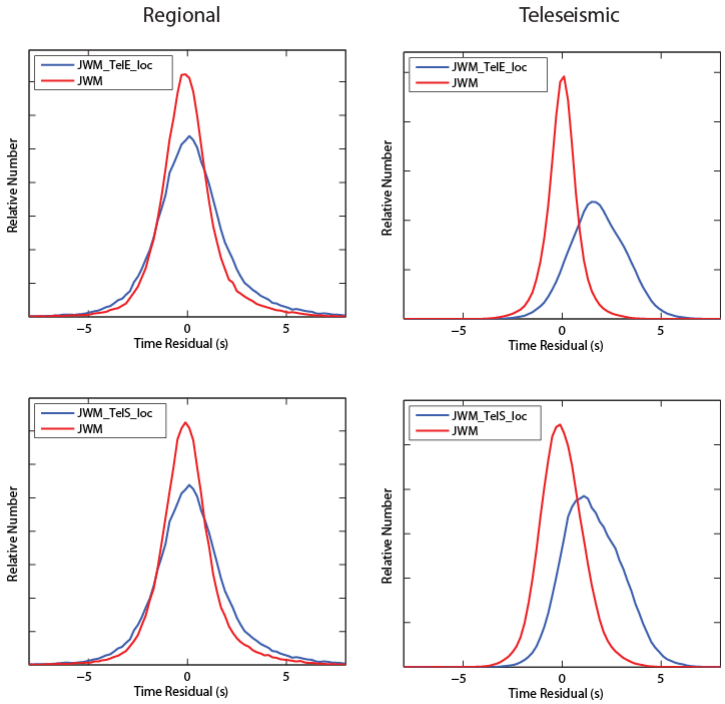

Figure 8. ***Red lines*****: Distributions of regional (left) and teleseismic (right) travel-time residuals for models JWM_TelE_loc (top panels) and model JWM_TelS_loc (bottom panels).** ***Blue lines:*** **Analogous distributions for model JWM.**

CONCLUSIONS AND RECOMMENDATIONS

We continue to develop and improve the tools needed to perform event location and travel-time calibration with regional and teleseismic arrival-time data, based on a unified 3D Earth model for travel-time calculation. Our latest numerical raytracing experiments show that the errors in linearized teleseismic travel-time calculations are 0.5 s or less, which is adequate for location and calibration but large enough to warrant further effort on making the errors even smaller. The use of linearization for travel-time prediction vastly reduces the computational requirements of a unified approach.

Our latest tests of joint regional/teleseismic tomography confirm the value of this approach in generating a 3D Earth model that predicts consistent travel times for regional and teleseismic P waves. The tests also show that accounting for event mislocations in the tomographic procedure does affect the velocity model that results, implying that location uncertainty must be quantified accurately in order to properly resolve the location/velocity trade-off. The use of secondary seismic phases (e.g. surface reflections and S phases) may ultimately address this problem. We are attempting to increase the capacity of our tomography algorithm significantly in order to handle much larger, multiple-phase data sets in a desktop computing environment.

REFERENCES

Antolik, M., Y. J. Gu, G. Ekström and A. M. Dziewonski (2003). J362D28: a new joint model of compressional and shear velocity in the Earth's mantle, *Geophys. J. Int*, 153: 2, 443–466.

Engdahl, E. R., R. van der Hilst and R. Buland (1998). Global teleseismic earthquake relocation with improved travel times and procedures for depth determination, *Bull. Seismol. Soc. Am*. 88: 722–743.

Flanagan, M. P., S. C. Myers and K. D. Koper (2007). Regional travel-time uncertainty and seismic location improvement using a three-dimensional a priori velocity model, *Bull. Seismol. Soc. Am*. 97: 804–825.

Kennett, B. L. N., E. R. Engdahl and R. Buland (1995). Constraints on the velocity structure in the Earth from travel times, *Geophys. J. Int*. 122: 108–124.

Murphy, J. R., W. Rodi, M. Johnson, et al. (2005). Calibration of International Monitoring System (IMS) stations in central and eastern Asia for improved seismic event location, *Bull. Seismol. Soc. Am*. 95: 1535–1560.

Pavlis, G. L., and J. R. Booker (1980). The mixed discrete continuous inverse problem: application to the simultaneous determination of earthquake hypocenters and velocity structure, *J. Geophys. Res*. 85: 4801–4810.

Podvin, P., and I. Lecomte (1991). Finite difference computation of traveltimes in very contrasted velocity models: a massively parallel approach and its associated tools, *Geophys. J. Int*. 105: 271–284.

Rawlinson, N., and M. Sambridge (2004). Wave front evolution in strongly heterogeneous layered media using the fast marching method, *Geophys. J. Int*. 156L: 63–647.

Reiter, D. T., and W. L. Rodi (2009). Validated 3D velocity models in Asia from joint regional body- and surface-wave tomography. *Final Report*, Weston Geophysical Corporation, AFRL-RV-HA-TR-2009-1009.

Ritzwoller, M. H., N. M. Shapiro, M. P. Barmin and A. L. Levshin (2002). Global surface wave diffraction tomography, *J. Geophys. Res*. 107: doi: 10.1029/2002JB001777.

Rodi, W. L., D. T. Reiter, S. C. Myers and N. A. Simmons (2009). A unified approach to joint regional/teleseismic calibration and event location with a 3D Earth model, in *Proceedings of the 2009 Monitoring Research Review: Ground-Based Nuclear Explosion Monitoring Technologies*, LA-UR-09-05276, Vol. 1, pp. 399–407.

Ryaboy, V., D. R. Baumgardt, P. Firbas, et al. (2001). Application of 3-D crustal and upper mantle velocity model of North America for location of regional seismic events, *Pure and Appl. Geophys*. 158: 79–103.

Simmons, N. A., S. C. Myers, and G. Johannesson (2010). Global-scale P-wave tomography designed for accurate prediction of regional and teleseismic travel times for Middle East events, in preparation.

Simmons, N. A., S. C. Myers and A. Ramirez (2010). Multi-resolution seismic tomography based on recursive tessellation hierarchy, these Proceedings.

Spencer, C., and D. Gubbins (1980). Travel time inversion for simultaneous earthquake location and velocity structure determination in laterally varying media, *Geophys. J. R. Astr. Soc*. 63: 95–116.

Um, J., and C. H. Thurber (1987). A fast algorithm for two-point seismic ray tracing, *Bull. Seismol. Soc. Am*. 77: 972–986.

Yang, X. P., I. Bondàr, J. Bhattacharyya, et al. (2004). Validation of regional and teleseismic travel-time models by relocating ground-truth events, *Bull. Seismol. Soc. Am*. 94: 897–919.

Zhao, D., A. Hasegawa and S. Horiuchi (1992). Tomographic imaging of P and S wave velocity structure beneath Northeastern Japan, *J. Geophys. Res*. 97: B13, 19909–19928.

Zhao, D. and J. Lei (2004). Seismic ray path variations in a 3D global velocity model, *Phys. Earth. Planet. Int.* 141: 153–166.